PCCP

Accepted Manuscript

ROYAL SOCIETY OF CHEMISTRY

www.rsc.org/pccp

Adsorption Properties of Nitrogen Dioxide on Hybrid Carbon and Boron-Nitride Nanotubes

*Haining Liu and C. Heath Turner**

Department of Chemical and Biological Engineering, The University of Alabama, Tuscaloosa, AL 35487-0203

*To whom correspondence should be addressed: hturner@eng.ua.edu
205-348-1733 (phone)
205-348-7558 (fax)

Abstract

The properties of pristine carbon nanotubes (CNTs) can be modified in a number of different ways: covalent attachments, substitutional doping, induced defects, and non-covalent interactions with ligands. One unconventional approach is to combine CNTs with boron-nitride nanotubes (BNNTs) to form hybrid carbon and boron-nitride nanotube (CBNNT) materials. In this work, we perform a first-principles density functional theory study on the adsorption properties of NO_2 on CBNNT heterostructures. It is found that the adsorption of NO_2 is significantly increased on both zigzag CBNNT(8,0) and armchair CBNNT(6,6), as compared to either a pristine CNT or BNNT. For example, the chemisorption of NO_2 on CNT(8,0) is found to be endothermic, while the chemisorption of NO_2 on CBNNT(8,0) is an exothermic process with a very large binding energy of –27.74 kcal mol^{-1}. Furthermore, the binding of NO_2 on both CBNNT(8,0) and CBNNT(6,6) induces an increase in the conductivity of the nanotube. These characteristics indicate that the CBNNT heterostructures may have significant potential as an NO_2 sensor or as a catalyst for NO_2 decomposition reactions. Our calculations provide critical information for further evaluation, such as molecular-level adsorption simulations and microkinetic studies.

Keywords

carbon nanotube, boron-nitride nanotube, adsorption, nitrogen dioxide, gas sensor, DFT

1. Introduction

Recently, there has been considerable interest in investigating the properties of chemically-modified carbon nanotubes (CNTs).[1, 2] This is due to the fact that modified CNTs show remarkably different features compared to pristine CNTs, and these modifications can help CNT-based materials meet the performance demands of real-world applications in many electronic, solar, and electocatalytic technologies.[3-8] An effective approach is to add substitutional dopants (such as nitrogen or boron) to the CNT, since this can significantly modify the original electronic structure of the material. Recently, various experimental methods have been reported for synthesizing boron-doped[9, 10] and nitrogen-doped CNTs[11] using many techniques such as the substitutional reaction of B_2O_3,[12] arc discharge,[13] and aerosol chemical vapor deposition methods.[14]

Another possible approach to modify CNTs is to hybridize CNTs with other structurally and chemically compatible nanotubes, such as boron-nitride nanotubes (BNNTs). Although BNNTs and CNTs can adopt very similar structures, their electronic properties are fundamentally different. For example, BNNTs are insulators,[15] while CNTs can be either metallic or semiconducting, depending on their chirality.[16] Therefore, combining these two different nanotubes into a hybrid material may result in a new material platform with unique (and tunable) electronic, catalytic, and/or sensor properties. Indeed, various experimental approaches to synthesize such hybrid carbon and boron-nitride nanotubes (CBNNTs, Fig. 1) have been reported and reviewed in the literature.[17-21] In addition, many computational studies have been performed to investigate the fundamental electronic, energetic, geometric and gas molecule adsorption properties of these hybrid nanotubes.[22-28] We recently reported a first-principles density functional theory (DFT) study of the adsorption of O_2 on CBNNT materials.[28] It was found that CBNNT materials have an increased ability to adsorb O_2 versus either pristine CNT or BNNT, and the chemisorption of O_2 on the CBNNTs significantly increases the conductivity of the nanotubes. Hence, CBNNT materials are predicted to be a promising new material for catalytic or gas sensor applications.

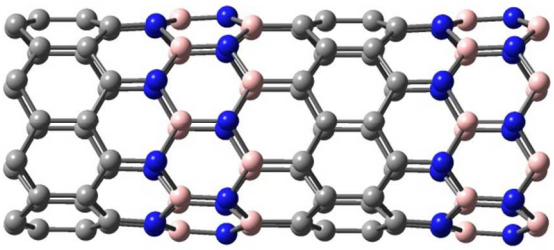

Fig. 1 The optimized structure of the CBNNT(8,0) model (with a diameter of ~6.4 Å) used in this study. Color scheme: Grey = carbon, blue = nitrogen, pink = boron.

Another industrially-relevant gas molecule is NO_2. It is a major air pollutant produced by automotive engines, fossil fuel combustion, and many manufacturing industries. Furthermore, NO_2 is able to react with and decompose ozone into O_2,[29] causing serious environmental concerns of atmospheric ozone depletion. Therefore, effective approaches for high-sensitivity detection and removal of NO_2 have attracted considerable interest. Many transition metals and metal oxides have been found to be able to adsorb and decompose NO_2.[30-35] Furthermore, carbon nanotubes have also been known to be able to interact with NO_2, which can cause changes in the electric resistance of the nanotube.[36] Currently, many NO_2 sensors are commercially available. However, there are a number of drawbacks in their low selectivity, limited sensitivity, and bulky size.[37] As a result, it is important to search for new NO_2-sensitive materials with better functionality. Although CBNNTs show an enhanced ability to adsorb O_2 compared to pristine CNTs and BNNTs[28] and the adsorptions of other relevant NO_x molecules on carbon nanomaterials have been studied as well,[38, 39] the interactions of CBNNT with NO_2 are completely unknown.

Finally, we note that NO_2 can form the NO_2 dimer (N_2O_4) at room temperature. However, due to the fact that NO_2 dimerization is an exothermic process, higher temperatures significantly inhibit the formation of N_2O_4. Since NO_2 is largely produced from combustion, typical high-temperature exhaust gas contains negligible amounts of the NO_2 dimer. As a result,

understanding the interaction of a single NO_2 with CBNNT will be most relevant to the majority of NO_2 sensor applications.

In this work, our CBNNT model is formed by a 1:1 stoichiometric combination of CNT and BNNT segments, which has been previously predicted to be a thermodynamically stable structure.[24] Using DFT calculations, the adsorption (chemisorption and physisorption) of NO_2 is studied on both zigzag (8,0) and armchair (6,6) CBNNT models, and the adsorption behavior is compared with that of pristine CNT and BNNT models. The adsorption calculations provide critical energetic information, which can be used in future molecular-level simulations of adsorption/selectivity, as well as microkinetic modeling of adsorption and reaction. In addition, the electronic structure characteristics of the CBNNT materials are characterized by analyzing the band structure and density of states upon adsorption of NO_2.

2. Computational Methods

In this work, our computational methods are similar to those used previously to model CBNNT$\cdots O_2$ interactions.[28] Specifically, the Vienna ab initio simulation package (VASP)[40-43] was used in all the calculations. The generalized gradient approximation (GGA) functional of Perdew, Burke, and Ernzerhof (PBE),[44] combined with the projector-augmented wave (PAW)[45, 46] method was used for geometry optimizations, with a 400 eV energy cutoff for the plane-wave basis set. For CBNNT(8,0), the dimensions of the unit cell are 19.37 Å × 19.57 Å × 8.69 Å with $\alpha = \beta = 90°$ and $\gamma = 120°$, while for CBNNT(6,6) the dimensions of the unit cell are 16.73 Å × 16.91 Å × 7.51 Å with $\alpha = \beta = 90°$ and $\gamma = 120°$. The Brillouin-zone integration was sampled by 1×1×3 *k*-points using the Monhorst-Pack scheme.[47] The density of states (DOS) and the band gap were obtained using a finer 1×1×11 *k*-point grid. The binding energy (*BE*) is obtained according to the following definition:

$$BE = E(NO_2/\text{Tube}) - E(NO_2) - E(\text{Tube}) \quad (1)$$

where $E(NO_2)$, E(Tube), and $E(NO_2/Tube)$ are the energies of an isolated NO_2 molecule, an isolated nanotube (CBNNT, CNT, or BNNT), and the NO_2/nanotube complex, respectively. Thus, a negative binding energy indicates a thermodynamically-favored exothermic adsorption process. Because NO_2 is a radical, all of the calculations were performed using the spin-polarized method in the doublet spin state. It is known that GGA functionals tend to underestimate adsorbate binding energies due to their poor description of dispersion interactions. Thus, in order to estimate the magnitude of the dispersion interaction (for selected structures), we performed single-point calculations using the DFT-D2 method developed by Grimme.[48] Partial charges were calculated by the Bader charge analysis.[49-51]

3. Results and discussion

3.1 Adsorption of NO_2 on CBNNT(8,0)

Nine chemisorbed NO_2/CBNNT(8,0) complexes were found in our study, with the CBNNT$\cdots NO_2$ interaction distances within the range of ~1.4–1.6 Å. The optimized structures with the calculated binding energies and key interaction distances are shown in Fig. 2. Previous studies on the interaction of NO_2 with CNT[52] and BNNT[53] found three possible configurations when NO_2 interacts with the nanotubes, which have been identified as:

a) *nitrite* configuration: an oxygen atom of NO_2 interacting with the nanotube;

b) *nitro* configuration: a nitrogen atom of NO_2 interacting with the nanotube; and

c) *cycloaddition* configuration: both oxygen atoms of NO_2 interacting with the nanotube.

Similarly, all these configurations were found in the NO_2/CBNNT(8,0) complexes. Furthermore, NO_2 can also interact with the BNNT component (NO_2/CBNNT(8,0)-1 to -5) or the CNT component (NO_2/CBNNT(8,0)-6 to -9) via the oxygen or nitrogen atom of NO_2 interacting with the boron or carbon atom of BCNNT. Interactions that involve the nitrogen atom of BCNNT could not be obtained. When NO_2 interacts with the BNNT component, the binding is found to be a highly exothermic process. The lowest energy structure, NO_2/CBNNT(8,0)-1 is in the nitrite configuration, and it has a calculated binding energy of –27.74 kcal mol^{-1}. The Bader

charge analysis shows that NO_2 carries a partial negative charge of –0.69, indicating a sizable charge transfer from the nanotube to NO_2 during the formation of this complex. As for the nitro configurations (NO_2/CBNNT(8,0)-4 and NO_2/CBNNT(8,0)-5), they are all found to be less energetically favorable than the nitrite configurations (NO_2/CBNNT(8,0)-1 to -3) by ~4–9 kcal mol^{-1}. In contrast, when NO_2 interacts with the CNT component, the binding is generally found to be endothermic. An exception is NO_2/CBNNT(8,0)-6, which is marginally thermoneutral with a very small binding energy of –0.09 kcal mol^{-1}. The binding energies of NO_2/CBNNT(8,0)-7 to -9 are all positive, suggesting that the formation of these chemisorbed complexes is not thermodynamically favored. The NO_2/CBNNT(8,0)-9 complex is the only cycloaddition configuration found in our study. However, the formation of this complex is the most endothermic with a calculated binding energy of 20.71 kcal mol^{-1}.

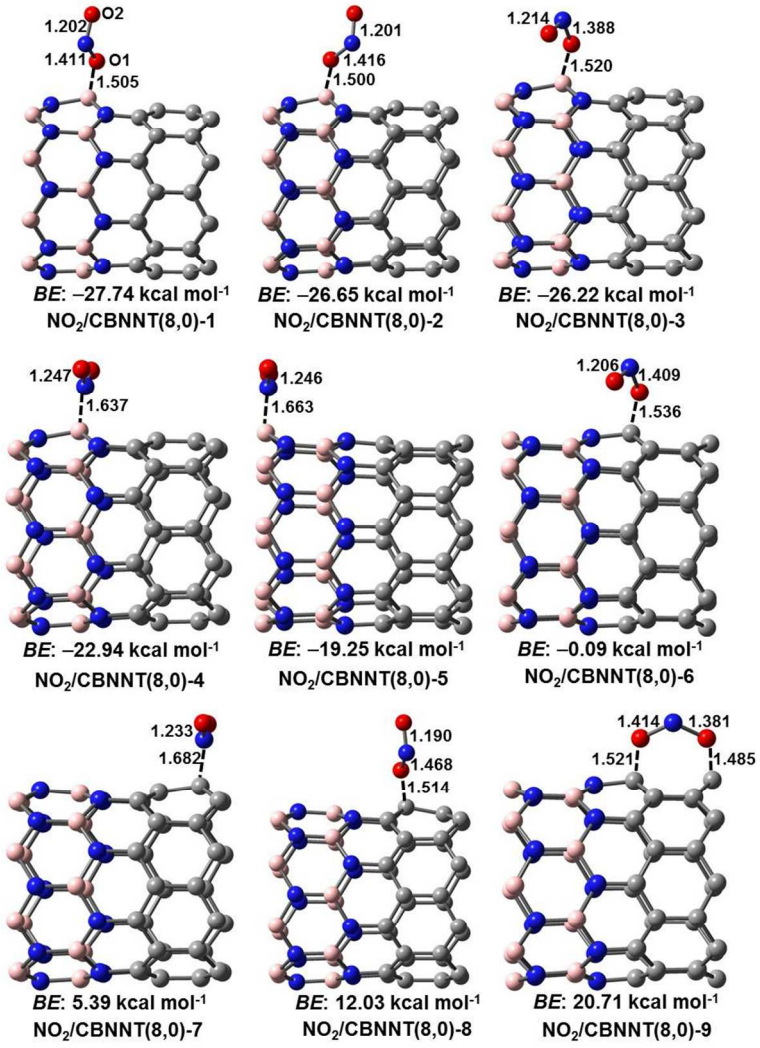

Fig. 2 The optimized structures of the chemisorbed NO_2/CBNNT(8,0) complexes. Key distances are shown in angstroms and colors are consistent with Fig. 1. The strongest chemisorption energy is observed in NO_2/CBNNT(8,0)-1 with a calculated BE of –27.74 kcal mol^{-1}.

As NO_2 interacts with CBNNT(8,0) in the nitrite configuration, the N–O bond which is directly involved in the interaction is found to be significantly lengthened. This in turn slightly distorts the other N–O bond (either slightly shortened or essentially remains unchanged). For example, the N–O1 and N–O2 bond lengths in NO_2/CBNNT(8,0)-1 are 1.411 and 1.202 Å, respectively. Compared to the N–O bond in free NO_2 which is calculated to be 1.214 Å at the same level of theory, the former is significantly lengthened by 0.197 Å while the latter is slightly

shortened by 0.012 Å. Such lengthening of the N–O bond (0.197 Å) is more significant than the adsorption of NO_2 on the ZnO surface (~0.04 Å)[54] and Pt surface (~0.1 Å),[55] but less significant than that on CNT, in which the N–O bond can be lengthened up to 1.457 Å.[52] In contrast to the nitrite configuration, for the nitro and the cycloaddition configurations, the interactions between NO_2 and CBNNT(8,0) cause the lengthening of both of the N–O bonds (see Fig. 2). For example, in the most stable nitro configuration complex NO_2/CBNNT(8,0)-4 the N–O bond is lengthened to a value of 1.247 Å, while in the cycloaddition complex NO_2/CBNNT(8,0)-9 a more considerable lengthening of the N–O bonds to 1.381 and 1.414 Å is observed. As found in a number of previous studies[56-59] on catalytic NO_2 decomposition reactions, the initial NO_2 adsorption on the catalytic surfaces often results in a lengthening of the N–O bond. Hence, the elongation of the N–O bond upon adsorption on CBNNT implies that CBNNT may also be a potential catalyst for NO_2 decomposition reactions.

We then considered the physisorbed NO_2/BCNNT complexes. Five complexes were found, and their optimized structures are shown in Fig. 3. Similar to the chemisorbed complexes, NO_2 can bind in the nitrite (NO_2/CBNNT(8,0)-10, NO_2/CBNNT(8,0)-12 and NO_2/CBNNT(8,0)-14), nitro (NO_2/CBNNT(8,0)-11), and cycloaddition (NO_2/CBNNT(8,0)-13) configurations. The interaction distances in the physisorbed complexes are much longer than those in the chemisorbed complexes, which results in much weaker binding energies. For example, the most stable physisorbed complex NO_2/CBNNT(8,0)-10 has a calculated binding energy of –3.05 kcal mol^{-1}, which is 24.69 kcal mol^{-1} weaker than the most stable chemisorbed complex NO_2/CBNNT(8,0)-1. In addition, the N–O bond in NO_2 is lengthened as in the chemisorbed complexes, but to a lesser extent. Furthermore, the charge transferred from the nanotube to NO_2 is also much less significant than that in NO_2/CBNNT(8,0)-1, as evidenced by the much smaller partial negative charge of –0.26 on NO_2 in NO_2/CBNNT(8,0)-10. This also suggests that in this configuration NO_2 has a much weaker interaction with CBNNT, as compared to the chemisorbed complex NO_2/CBNNT(8,0)-1.

As the GGA functional that is used is unable to properly describe the dispersion interactions (which are relevant to weakly-bound physisorbed complexes), we performed single-point calculations on the lowest energy physisorbed complex NO_2/CBNNT(8,0)-10 using the DFT-D2 method. The calculated binding energy with dispersion corrections is –5.52 kcal mol^{-1}, which indicates an underestimate of 2.47 kcal mol^{-1} to the binding energy using the GGA functional. A previous study[60] on the interaction of O_2 with BNNT(5,5) found a very consistent dispersion interaction (with only ~0.2 kcal mol^{-1} difference amongst all of the physisorbed complexes). Hence, we expect a similar trend for the physisorbed complexes in this study.

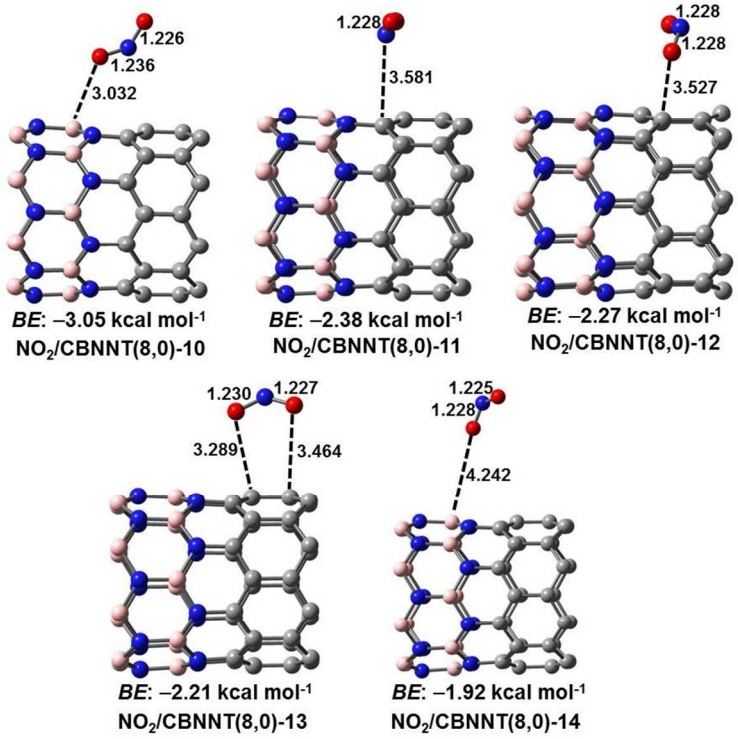

Fig. 3 The optimized structures of the physisorbed NO_2/CBNNT(8,0) complexes. Key distances are shown in angstroms and colors are consistent with Fig. 1. The strongest physisorption energy is observed in NO_2/CBNNT(8,0)-10 with a calculated BE of –3.05 kcal mol^{-1}.

In order to compare the binding of NO_2 on CBNNT(8,0) with that on the pristine CNT and BNNT, the NO_2/CNT(8,0) and NO_2/BNNT(8,0) complexes were also investigated. The binding

of NO_2 with various zigzag and armchair CNTs have been thoroughly addressed in previous studies.[52, 61-69] Several chemisorbed complexes of a single NO_2 molecule on CNT(8,0) were obtained,[52] all with positive binding energies (endothermic process) in the range of 1.3–30.4 kcal mol^{-1} using the GGA functional PW91 with the Vanderbilt ultrasoft pseudopoential in VASP. In our work, we obtained only one chemisorbed NO_2/CNT(8,0) complex in the nitrite configuration with an endothermic binding energy of 13.00 kcal mol^{-1} (Fig. 4). This is significantly different from the hybrid CBNNT, in which the most stable chemisorbed NO_2/CBNNT(8,0)-1 complex has a negative binding energy (exothermic process) of –27.74 kcal mol^{-1}. Although the chemisorption of a single NO_2 molecule on CNT was found to be endothermic, the chemisorption of a second NO_2 molecule on CNT(8,0) was found to be exothermic with the highest binding energy value of –21.4 kcal mol^{-1}, with respect to the sum of the energies of a singly-adsorbed complex (NO_2/CBNNT(8,0)) and a free NO_2 molecule.[52] This result was attributed to the formation of a radical on the nanotube upon the adsorption of the first NO_2 molecule, which then makes the interaction with another NO_2 radical a thermodynamically favored process.[52] However, the calculated binding energy of a second NO_2 on a singly-absorbed NO_2/CNT(8,0) complex is still weaker than the NO_2/CBNNT(8,0) binding energy obtained in our study. Furthermore, if a second NO_2 molecule adsorbs on CBNNT, its binding energy is similarly expected to be much stronger than that of the first NO_2 molecule.

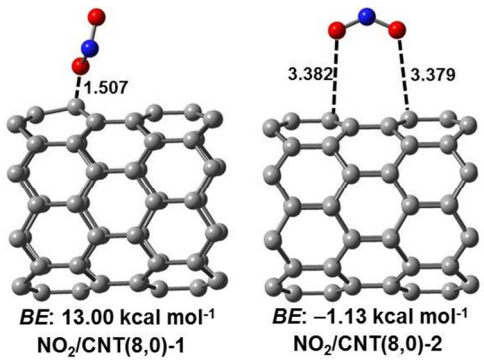

Fig. 4 The optimized structures of a chemisorbed complex NO_2/CNT(8,0)-1 and the lowest energy physisorbed complexes NO_2/CNT(8,0)-2. Key distances are shown in angstroms and colors are consistent with Fig. 1.

In addition to the chemisorbed NO_2/CNT complex, we obtained three physisorbed NO_2/CNT(8,0) complexes. The optimized structure of the most stable physisorbed complex NO_2/CNT(8,0)-2 is shown in Fig. 4, while the other two complexes (slightly higher in energy) are shown in ESI. The NO_2/CNT(8,0)-2 complex has a calculated binding energy of –1.13 kcal mol^{-1}, which is weaker than the physisorbed NO_2/CBNNT(8,0) complexes. As a result, the hybrid CBNNT(8,0) shows an increased NO_2 adsorption strength by approximately 29 kcal mol^{-1}, as compared with pristine CNT(8,0).

For the adsorption of NO_2 on pristine BNNT, eight complexes were obtained in our study. The most stable chemisorbed and physisorbed complexes are shown in Fig. 5, while all the rest of the structures are shown in ESI. Similar to CNT(8,0), the chemisorption of NO_2 on BNNT(8,0) is found to be an endothermic process with a calculated binding energy of 10.77 kcal mol^{-1}. Furthermore, the binding energy of the physisorbed NO_2/BNNT(8,0) complex of –0.74 kcal mol^{-1} is also weaker than that of the lowest energy physisorbed NO_2/CBNNT(8,0) complex by 2.31 kcal mol^{-1}. As a result, the hybrid CBNNT(8,0) also increases the NO_2 binding strength as compared to the pristine BNNT.

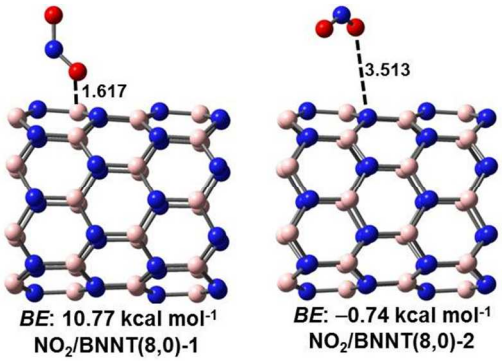

Fig. 5 The optimized structures of the lowest energy chemisorbed complex NO_2/BNNT(8,0)-1 and the lowest energy physisorbed complex NO_2/BNNT(8,0)-2. Key distances are shown in angstroms and colors are consistent with Fig. 1.

3.2 Adsorption of NO_2 on CBNNT(6,6)

The optimized structures of the chemisorbed NO_2/CBNNT(6,6) complexes are shown in Fig. 6. Only the nitrite (NO_2/CBNNT(6,6)-1, -2, -3 and -5) and nitro (NO_2/CBNNT(6,6)-4) configurations could be obtained. The NO_2/CBNNT(6,6)-1 complex has the strongest binding energy of –8.03 kcal mol^{-1}. However, it is still 19.71 kcal mol^{-1} weaker than that of NO_2/CBNNT(8,0)-1. Similar to NO_2/CBNNT(8,0)-1, a charge transfer is observed from the nanotube to NO_2, with a calculated Bader charge on NO_2 of –0.67 in NO_2/CBNNT(6,6)-1, which is slightly less negative than that in NO_2/CBNNT(8,0)-1 (–0.69). This smaller charge transfer may be attributed in part to the smaller band gap of CBNNT(8,0) (0.98 eV) versus CBNNT (6,6) (1.40 eV). This, therefore, results in a weaker binding of NO_2 with CBNNT(6,6) than with CBNNT(8,0). The NO_2 molecules in NO_2/CBNNT(6,6)-1 to -4 interact with a boron atom from CBNNT, and the negative binding energies suggest that the formation of these complexes is thermodynamically favored. In contrast, NO_2 in NO_2/CBNNT(6,6)-5 interacts with a carbon atom, and the calculated binding energy is a large positive value of 17.09 kcal mol^{-1}.

Similar to the NO_2/CBNNT(8,0) complexes, the N–O bond which is directly involved in the interaction with CBNNT is found to be significantly lengthened. For example, the N–O1 bond in NO_2/CBNNT(6,6)-1 is calculated to be 1.348 Å, which is 0.134 Å longer than that in the free NO_2. In contrast, the N–O2 bond in NO_2/CBNNT(6,6)-1 only marginally increases by 0.005 Å to 1.219 Å. In general, the lengthening of the N–O bond in the NO_2/CBNNT(6,6) complexes is less significant than that in the NO_2/CBNNT(8,0) complexes. This observation corresponds with the fact that NO_2 binds weaker with CBNNT(6,6) than with CBNNT (8,0).

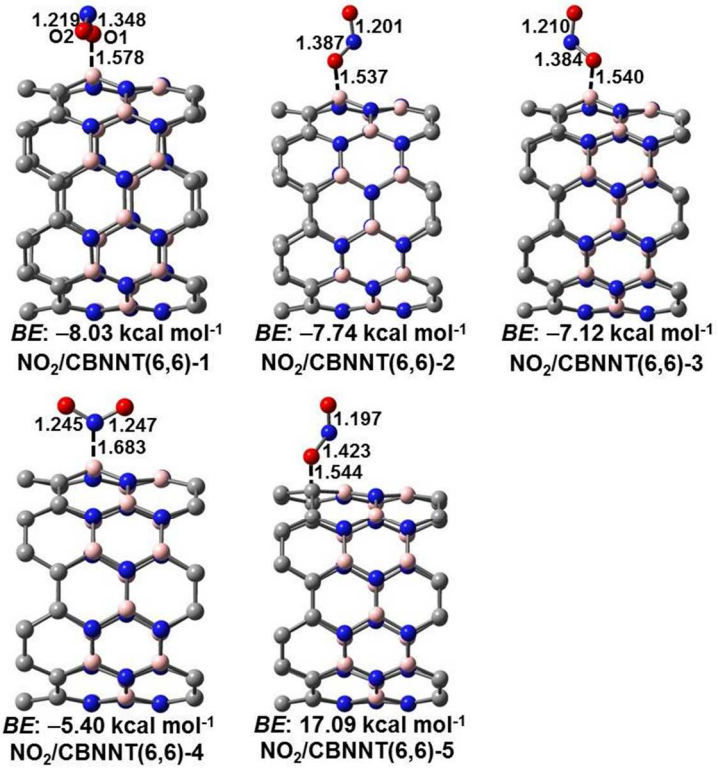

Fig. 6 The optimized structures of the chemisorbed NO_2/CBNNT(6,6) complexes. Key distances are shown in angstroms and colors are consistent with Fig. 1. The strongest chemisorption energy is observed in NO_2/CBNNT(6,6)-1 with a calculated BE of –8.03 kcal mol^{-1}.

Several physisorbed NO_2/CBNNT(6,6) complexes were also obtained with the optimized structures shown in Fig. 7. The interaction distances are much longer than the chemisorbed NO_2/CBNNT(6,6) complexes. As a result, the binding energies of the physisorbed NO_2/CBNNT(6,6) complexes are much weaker than the chemisorbed NO_2/CBNNT(6,6) complexes. For example, the lowest energy physisorbed complex NO_2/CBNNT(6,6)-6 has a calculated binding energy of only –1.87 kcal mol^{-1}. Such a weak binding between NO_2 and the nanotube results in much smaller charge transfer, with the calculated Bader charge on NO_2 of only –0.19 in NO_2/CBNNT(6,6)-6.

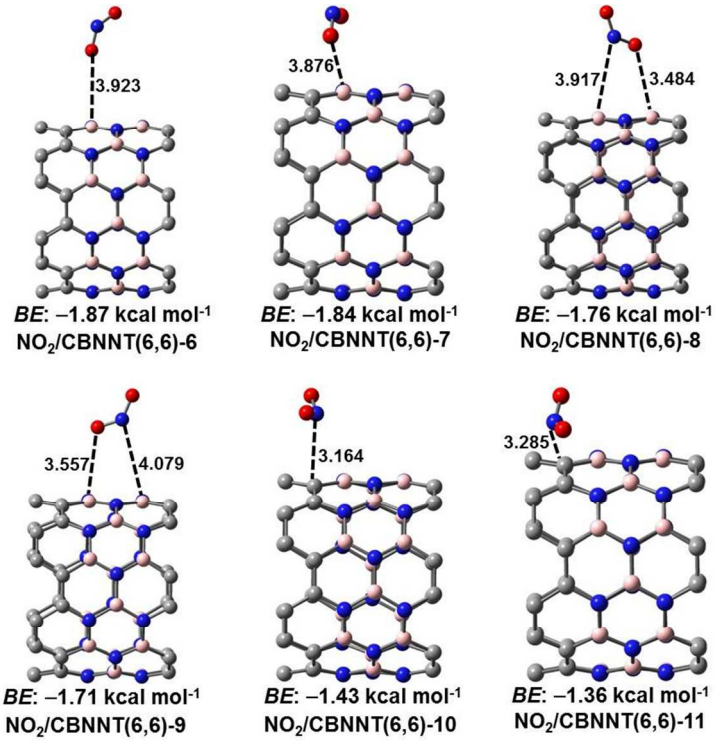

Fig. 7 The optimized structures of the physisorbed NO_2/CBNNT(6,6) complexes. Key distances are shown in angstroms and colors are consistent with Fig. 1. The strongest physisorption energy is observed in NO_2/CBNNT(6,6)-6 with a calculated BE of –1.87 kcal mol^{-1}.

Similar to the NO_2/CBNNT(8,0) complex, we also performed single-point calculations on lowest energy physisorbed complex NO_2/CBNNT(6,6)-6 using the DFT-D2 method to account for the magnitude of the dispersion interaction. The calculated binding energy of NO_2/CBNNT(6,6)-6 with dispersion correction is –3.74 kcal mol^{-1}, which is only 1.87 kcal mol^{-1} stronger than that without the inclusion of dispersion interaction. As a result, a consistent ~2 kcal mol^{-1} underestimate of the binding energy for the physisorbed NO_2/CBNNT(8,0) and NO_2/CBNNT(6,6) complexes is expected due to the inadequate description of dispersion interactions by the GGA functional.

The binding characteristics of NO_2 on pristine CNT(6,6) and BNNT(6,6) were also investigated to compare with the NO_2 binding on CBNNT(6,6). Only physisorbed NO_2/CNT(6,6)

and NO_2/BNNT(6,6) complexes could be obtained in our study. The lowest energy NO_2/CNT(6,6) and NO_2/BNNT(6,6) complexes are shown in Fig. 8, and all of the obtained complexes are provided in ESI. The binding energy of NO_2/CNT(6,6)-1 is a positive value of 3.97 kcal mol^{-1}, suggesting that it is a thermodynamically unfavored adsorption complex. In addition, the binding energy of NO_2/BNNT(6,6)-1 is only slightly negative at a value of –0.61 kcal mol^{-1}, which is 7.42 kcal mol^{-1} weaker than that of the lowest energy NO_2/CBNNT(6,6) complex. Therefore, similar to the (8,0) analogue, the hybrid CBNNT(6,6) also shows an increased ability to bind NO_2, as compared with pristine CNT(6,6) and BNNT(6,6).

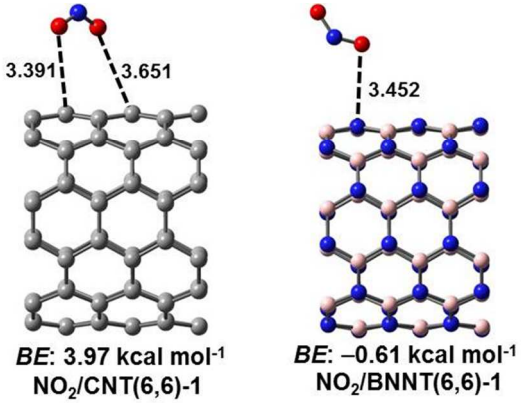

Fig. 8 The optimized structures of the lowest energy NO_2/CNT(6,6) and NO_2/BNNT(6,6) complexes. Key distances are shown in angstroms and colors are consistent with Fig. 1.

In addition to the comparisons with pristine CNT and BNNT, the binding of NO_2 on CBNNT is also stronger than many of the structurally defective and heteroatom-doped CNT models. For instance, binding energies can be compared against CNT models with Stone-Wales defects (*BE* = –20.99 kcal mol^{-1}),[70] B-doped CNTs (*BE* = –24.21 kcal mol^{-1})[71] and N-doped CNTs (*BE* = –13.61 kcal mol^{-1}),[71] monovacancy defective CNTs (*BE* = –65.95 kcal mol^{-1}),[70] Co-doped CNTs (*BE* = –54.36 kcal mol^{-1}),[72] Rh-doped CNTs (*BE* = –47.95 kcal mol^{-1}),[72] Ir-doped CNTs (*BE* = –60.41 kcal mol^{-1})[72] and Si-C nanotubes (*BE* = –32.52 kcal mol^{-1}).[73] It is worth noting that the binding energy of NO_2/CBNNT(8,0)-1 is comparable to the computed binding energy of NO_2 on

B-doped CNT(10,0) (–24.21 kcal mol^{-1}) reported in the literature.[71] This is likely due to the preference of boron within the CBNNT to interact with the NO_2 adsorbate. Such a strong B···O interaction between NO_2/CBNNT(8,0)-1 can also be seen from the projected density of states (provided in ESI), which shows significant overlap between the O-p and B-p states. Hence, in the most stable NO_2/CBNNT(8,0) complex, the hybrid CBNNT nanotube seems to show similar adsorption characteristics to a boron doped CNT. However, a primary advantage of the CBNNT materials is that the band gap of the nanotube can be methodically tuned by varying the ratio of the CNT and BNNT components[24]. In principle, this tunability should modulate the charge transfer ability of the CBNNT, which may be able to further alter its binding energy with NO_2. Indeed, we tested another CBNNT(8,0) nanotube formed by a 2:2 stoichiometric combination of CNT and BNNT segments. By using the same NO_2 orientation as that in NO_2/CBNNT(8,0)-1, the binding energy was calculated to be –39.64 kcal mol^{-1}, which is 11.90 kcal mol^{-1} stronger than that of NO_2/CBNNT(8,0)-1 (the calculated total density of states is provided in ESI). Hence, this preliminary result shows the great potential to further tune the CBNNT···NO_2 binding energy by using different types of CBNNTs.

3.3 Electronic structures

In order to further investigate the influence of the NO_2 binding on the electronic properties of CBNNT, the band structures and the total density of states (DOS) of the lowest energy chemisorbed and physisorbed NO_2/CBNNT(8,0) and NO_2/CBNNT(6,6) complexes are shown in Fig. 9. As a comparison, the pristine CBNNT(8,0) and CBNNT(6,6) materials are semiconductors, with calculated band gaps (direct) of 0.98 and 1.40 eV, respectively. When NO_2 is chemisorbed onto CBNNT(8,0), the calculated band gap decreases to 0.16 eV. Furthermore, significant electron densities are populated at the Fermi level as observed from the total DOS. All of these observations suggest that the conductivity significantly increases in the chemisorbed complex NO_2/CBNNT(8,0)-1. A similar conductivity increase is also observed in the physisorbed complex NO_2/CBNNT(8,0)-10, which has a calculated band gap of 0.09 eV. When

NO_2 binds with CBNNT(6,6), both the chemisorbed and physisorbed complexes become metallic, as can be seen from the band crossing the Fermi level in the band structures shown in Figure 9. All of these results indicate that NO_2 is able to increase the conductivity of the hybrid CBNNT(8,0) and (6,6). This is similar to the behavior predicted for CNT from both computations[52, 66] on a series of zigzag CNTs from (7,0) to (12,0) and experiment on semiconducting chiral CNTs[36] and BNNT(8,0), with calculated band gaps that decreased from 5.63 to 3.12 eV.[53] Such conductivity increase suggests that such hybrid nanotubes may have potential applications as an NO_2 sensor.

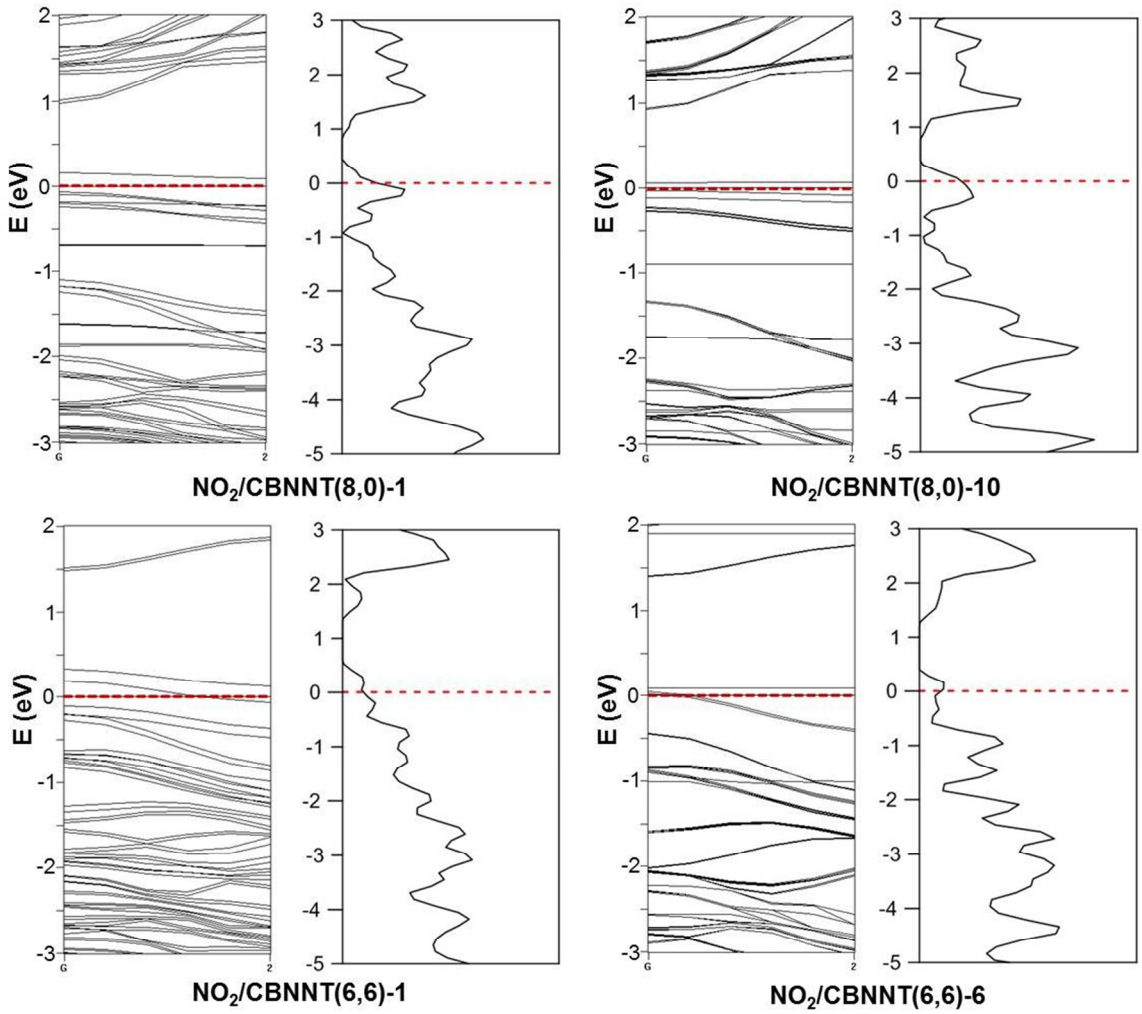

Fig. 9 The calculated band structures and total density of states for the lowest energy chemisorbed and physisorbed NO_2/CBNNT(8,0) and NO_2/CBNNT(6,6) complexes. The Fermi level (red line) is shifted to 0 eV.

4. Conclusions

In this work, DFT methods have been used to investigate the ability of hybrid carbon and boron-nitride carbon nanotubes to adsorb and potentially detect NO_2. It is found that both the zigzag CBNNT(8,0) and armchair CBNNT(6,6) show a significantly enhanced ability to adsorb NO_2 compared with pristine CNTs and BNNTs. For example, the lowest energy chemisorbed NO_2/CBNNT(8,0) complex has a calculated binding energy of –27.74 kcal mol^{-1}. In contrast, similar to a previous study,[52] the chemisorption of NO_2 on CNT(8,0) is found to be endothermic, with a positive binding energy of 13.00 kcal mol^{-1}, and the calculated binding energy of the physisorbed NO_2/CNT(8,0) complex is slightly exothermic at only –1.13 kcal mol^{-1}. The binding of NO_2 on CBNNT(6,6) is found to be weaker than that on CBNNT(8,0), but as a comparison, it is considerably stronger than the binding on pristine CNT(6,6) and BNNT(6,6). Furthermore, it is found that the binding of NO_2 on CBNNT(8,0) and CBNNT(6,6) results in a significant bond distortion of the NO_2 molecule and an increase in the conductivity of the nanotube, suggesting that these hybrid nanotubes may be useful as a catalyst for NO_2 decomposition reactions or in sensing applications. Together with our previous study[28] that showed CBNNT strongly adsorbs O_2 (compared with pristine CNT and BNNT), this opens attractive possibilities of using CBNNT as a new material in gas sensor, electrochemical, and catalytic applications. This work should motivate further experimental investigations of these materials, as well as provide critical energetic information for larger-scale simulation studies.

Acknowledgment We appreciate the computational resources of the Alabama Supercomputer Authority. Partial financial support was provided by The University of Alabama Research Stimulation Fund and the National Science Foundation (CBET-0747690).

Electronic supplementary information (ESI) available: The optimized structures of the NO_2/CNT(8,0) NO_2/BNNT(8,0), NO_2/CNT(6,6) and NO_2/BNNT(6,6) complexes obtained in this study. The calculated projected density of states of NO_2/CBNNT(8,0)-1. The calculated total density of states for the complex between NO_2 and a CBNNT with a 2:2 stoichiometric combination of CNT and BNNT segments.

References

1. U. N. Maiti, W. J. Lee, J. M. Lee, Y. Oh, J. Y. Kim, J. E. Kim, J. Shim, T. H. Han and S. O. Kim, *Adv. Mater.*, 2013, **26**, 40-67.
2. G. G. Wildgoose, C. E. Banks, H. C. Leventis and R. G. Compton, *Microchim. Acta*, 2006, **152**, 187-214.
3. J. P. Paraknowitsch and A. Thomas, *Energy & Environmental Science*, 2013, **6**, 2839-2855.
4. D.-W. Wang and D. Su, *Energy & Environmental Science*, 2014, **7**, 576-591.
5. L. Yang, S. Jiang, Y. Zhao, L. Zhu, S. Chen, X. Wang, Q. Wu, J. Ma, Y. Ma and Z. Hu, *Angew. Chem. Int. Ed.*, 2011, **50**, 7132-7135.
6. N. Daems, X. Sheng, I. F. J. Vankelecom and P. P. Pescarmona, *J. Mater. Chem. A*, 2014, **2**, 4085-4110.
7. Z. Yang, H. Nie, X. A. Chen, X. Chen and S. Huang, *J. Power Sources*, 2013, **236**, 238-249.
8. X. Q. Zhang, H. Li and K. M. Liew, *J. Appl. Phys.*, 2007, **102**, 073709.
9. K. McGuire, N. Gothard, P. L. Gai, M. S. Dresselhaus, G. Sumanasekera and A. M. Rao, *Carbon*, 2005, **43**, 219-227.
10. F. H. Monteiro, D. G. Larrude, M. E. H. Maia da Costa, L. A. Terrazos, R. B. Capaz and F. L. Freire, *J. Phys. Chem. C*, 2012, **116**, 3281-3285.
11. P. Ayala, R. Arenal, M. Rummeli, A. Rubio and T. Pichler, *Carbon*, 2010, **48**, 575-586.
12. W. Han, Y. Bando, K. Kurashima and T. Sato, *Chem. Phys. Lett.*, 1999, **299**, 368-373.
13. W. K. Hsu, S. Firth, P. Redlich, M. Terrones, H. Terrones, Y. Q. Zhu, N. Grobert, A. Schilder, R. J. H. Clark, H. W. Kroto and D. R. M. Walton, *J. Mater. Chem.*, 2000, **10**, 1425-1429.
14. A. A. Koos, M. Dowling, K. Jurkschat, A. Crossley and N. Grobert, *Carbon*, 2009, **47**, 30-37.
15. X. Blase, A. Rubio, S. G. Louie and M. L. Cohen, *Europhys. Lett.*, 1994, **28**, 335-340.
16. J. W. G. Wilder, L. C. Venema, A. G. Rinzler, R. E. Smalley and C. Dekker, *Nature*, 1998, **391**, 59-62.
17. K. Suenaga, C. Colliex, N. Demoncy, A. Loiseau, H. Pascard and F. Willaime, *Science*, 1997, **278**, 653-655.
18. S. Enouz, O. Stephan, J.-L. Cochon, C. Colliex and A. Loiseau, *Nano Lett.*, 2007, **7**, 1856-1862.
19. W. L. Wang, X. D. Bai, K. H. Liu, Z. Xu, D. Golberg, Y. Bando and E. G. Wang, *J. Am. Chem. Soc.*, 2006, **128**, 6530-6531.
20. X. Wei, M.-S. Wang, Y. Bando and D. Golberg, *ACS Nano*, 2011, **5**, 2916-2922.
21. P. Ayala, R. Arenal, A. Loiseau, A. Rubio and T. Pichler, *Rev. Mod. Phys.*, 2010, **82**, 1843-1885.
22. Z.-Y. Zhang, Z. Zhang and W. Guo, *J. Phys. Chem. C*, 2009, **113**, 13108-13114.
23. Y. Fan, M. Zhao, T. He, Z. Wang, X. Zhang, Z. Xi, H. Zhang, K. Hou, X. Liu and Y. Xia, *J. Appl. Phys.*, 2010, **107**, 094304-094306.
24. W. An and C. H. Turner, *J. Phys. Chem. Lett.*, 2010, **1**, 2269-2273.
25. J. M. Pruneda, *Phys. Rev. B*, 2012, **85**, 045422.
26. A. Du, Y. Chen, Z. Zhu, G. Lu and S. C. Smith, *J. Am. Chem. Soc.*, 2009, **131**, 1682-1683.

27. V. V. Ivanovskaya, A. Zobelli, O. Stephan, P. R. Briddon and C. Colliex, *J. Phys. Chem. C*, 2009, **113**, 16603-16609.
28. H. Liu and C. H. Turner, *J. Comput. Chem.*, 2014, **35**, 1058-1063.
29. C. H. Wu, E. D. Morris and H. Niki, *J. Phys. Chem.*, 1973, **77**, 2507-2511.
30. C. Wesenberg, O. Autzen and E. Hasselbrink, *J. Chem. Phys.*, 2006, **125**, 224707.
31. J. Wang, M. R. Voss, H. Busse and B. E. Koel, *j. Phys. Chem. B*, 1998, **102**, 4693-4696.
32. J. A. McCleverty, *Chem. Rev.*, 1979, **79**, 53-76.
33. J. Wang and B. E. Koel, *J. Phys. Chem. A*, 1998, **102**, 8573-8579.
34. O. Autzen, C. Wesenberg and E. Hasselbrink, *Phys. Rev. Lett.*, 2006, **96**, 196807.
35. D. C. Sorescu, C. N. Rusu and J. T. Yates, *J. Phys. Chem. B*, 2000, **104**, 4408-4417.
36. J. Kong, N. R. Franklin, C. Zhou, M. G. Chapline, S. Peng, K. Cho and H. Dai, *Science*, 2000, **287**, 622-625.
37. A.-M. Andringa, C. Piliego, I. Katsouras, P. W. M. Blom and D. M. d. Leeuw, *Chem. Mater.*, 2014, **26**, 773-785.
38. Y.-a. Lv, G.-l. Zhuang, J.-g. Wang, Y.-b. Jia and Q. Xie, *Phys. Chem. Chem. Phys.*, 2011, **13**, 12472-12477.
39. X. Zhang, Z. Lu, Y. Tang, D. Ma and Z. Yang, *Catal. Lett.*, 2014, **144**, 1016-1022.
40. G. Kresse and J. Hafner, *Phys. Rev. B*, 1993, **47**, 558-561.
41. G. Kresse and J. Hafner, *Phys. Rev. B*, 1994, **49**, 14251-14269.
42. G. Kresse and J. Furthmuller, *Phys. Rev. B*, 1996, **54**, 11169-11186.
43. G. Kresse and J. Furthmuller, *Comput. Mat. Sci.*, 1996, **6**, 15-50.
44. J. P. Perdew, K. Burke and M. Ernzerhof, *Phys. Rev. Lett.*, 1996, **77**, 3865-3868.
45. P. E. Blochl, *Phys. Rev. B*, 1994, **50**, 17953-17979.
46. G. Kresse and D. Joubert, *Phys. Rev. B*, 1999, **59**, 1758-1775.
47. H. J. Monkhorst and J. D. Pack, *Phys. Rev. B*, 1976, **13**, 5188-5192.
48. S. Grimme, *J. Comput. Chem.*, 2006, **27**, 1787-1799.
49. G. Henkelman, A. Arnaldsson and H. Jónsson, *Comput. Mater. Sci.*, 2006, **36**, 254-360.
50. E. Sanville, S. D. Kenny, R. Smith and G. Henkelman, *J. Comput. Chem.*, 2007, **28**, 899-908.
51. W. Tang, E. Sanville and G. Henkelman, *J. Phys.: Condens. Matter*, 2009, **21**, 084204.
52. W.-L. Yim, X. G. Gong and Z.-F. Liu, *J. Phys. Chem. B*, 2003, **107**, 9363-9369.
53. P. Singla, S. Singhal and N. Goel, *Appl. Surface Sci.*, 2013, **283**, 881-887.
54. M. Breedon, M. J. S. Spencer and I. Yarovsky, *Surface Science*, 2009, **603**, 3389-3399.
55. R. B. Getman and W. F. Schneider, *J. Phys. Chem. C*, 2006, **111**, 389-397.
56. J. A. Rodriguez, T. Jirsak, G. Liu, J. Hrbek, J. Dvorak and A. Maiti, *J. Am. Chem. Soc.*, 2001, **123**, 9597-9605.
57. T. Jirsak, M. Kuhn and J. A. Rodriguez, *Surface Sci.*, 2000, **457**, 254-266.
58. N. Y. Dzade, A. Roldan and N. H. de Leeuw, *Phys. Chem. Chem. Phys.*, 2014, **16**, 15444-15456.
59. M. Sacchi, M. C. E. Galbraith and S. J. Jenkins, *Phys. Chem. Chem. Phys.*, 2012, **14**, 3627-3633.
60. J. Zhang, K. P. Loh, J. Zheng, M. B. Sullivan and P. Wu, *Phys. Rev. B*, 2007, **75**, 245301.
61. Z. Jijun, B. Alper, H. Jie and L. Jian Ping, *Nanotechnology*, 2002, **13**, 195.
62. A. Ricca and C. W. Bauschlicher Jr, *Chem. Phys.*, 2006, **323**, 511-518.
63. S. Peng and K. Cho, *Nanotechnology*, 2000, **11**, 57-60.
64. H. Chang, J. D. Lee, S. M. Lee and Y. H. Lee, *Appl. Phys. Lett.*, 2001, **79**, 3863-3865.

65. K. Seo, K. A. Park, C. Kim, S. Han, B. Kim and Y. H. Lee, *J. Am. Chem. Soc.*, 2005, **127**, 15724-15729.
66. Y. Zhang, C. Suc, Z. Liu and J. Li, *J. Phys. Chem. B*, 2006, **110**, 22462-22470.
67. J. Dai, P. Giannozzi and J. Yuan, *Surface Sci.*, 2009, **603**, 3234-3238.
68. S.-C. Hsieh, S.-M. Wang and F.-Y. Li, *Carbon*, 2011, **49**, 955-965.
69. S. Peng, K. Cho, P. Qi and H. Dai, *Chem. Phys. Lett.*, 2004, **387**, 271-276.
70. S. Tang and Z. Cao, *J. Chem. Phys.*, 2009, **131**, 14706.
71. L. Bai and Z. Zhou, *Carbon*, 2007, **45**, 2105-2110.
72. C. Tabtimsai, B. Wanno and V. Ruangpornvisuti, *Mater. Chem. Phys.*, 2013, **138**, 709-715.
73. B. Xiao, J.-x. Zhao, Y.-h. Ding and C.-C. Sun, *Surface Sci.*, 2010, **604**, 1882-1888.

Adsorption Properties of Nitrogen Dioxide on Hybrid Carbon and Boron-Nitride Nanotubes

Haining Liu and C. Heath Turner

Department of Chemical and Biological Engineering, The University of Alabama, Tuscaloosa, Alabama USA 35487-0203

Graphical Abstract

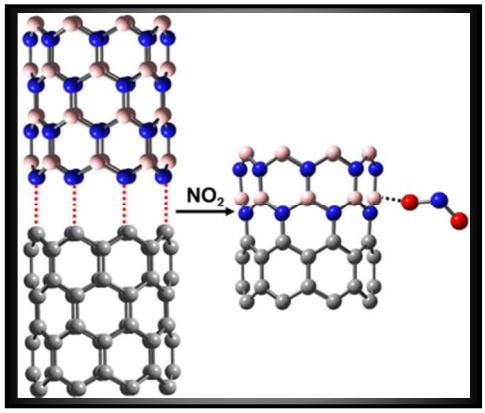

Hybrid CNT/BNNT materials are predicted to have enhanced NO_2 adsorption, which leads to large shifts in band gap, indicating potential sensing applications.